

Core-assisted gas capture instability: a new mode of giant planet formation by gravitationally unstable discs

Sergei Nayakshin¹, Ravit Helled² and Aaron C. Boley³

¹ *Department of Physics & Astronomy, University of Leicester, Leicester, LE1 7RH, UK. E-mail: Sergei.Nayakshin@le.ac.uk*

² *Department of Geophysics, Atmospheric, and Planetary Sciences, Tel-Aviv University, Israel.*

³ *The University of British Columbia, Department of Physics and Astronomy, 6224 Agricultural Rd., Vancouver, BC V6T 1Z1, Canada.*

Received

ABSTRACT

Giant planet formation in the core accretion plus gas capture (CA) paradigm is predicated by the formation of a core, assembled by the coagulation of grains and later by planetesimals within a protoplanetary disc. As the core mass increases beyond a critical value, the hydrogen-dominated atmosphere around the core becomes self-gravitating and collapses onto the core, triggering rapid gas accretion which can lead to the formation of a gaseous planet. In contrast, in the disc instability paradigm, giant planet formation is believed to be independent of core formation: massive self-gravitating gas fragments cool radiatively and collapse as a whole independently of whether there is a core.

In this paper we show that giant planet formation in the disc instability model may be also enhanced by core formation for reasons physically very similar to the CA paradigm. In the model explored here, efficient grain sedimentation within an initial fragment (rather than the disc) leads to the formation of a core composed of heavy elements. We find that massive atmospheres form around cores and undergo collapse as a critical core mass is exceeded, analogous to CA theory. The critical mass of the core to initiate such a collapse depends on the fragment mass and metallicity, as well as core luminosity, but ranges from less than 1 to as much as ~ 80 Earth masses. We therefore suggest that there are two channels for the collapse of a gaseous fragment to planetary scales within the disc instability model: (i) H_2 dissociative collapse of the entire gaseous clump, and (ii) core-assisted gas capture, as presented here. We suggest that the first of these two is favoured in metal-poor environments and for fragments $\gtrsim 5 - 10$ Jupiter masses, whereas the second is favored in metal-rich environments and fragments of lower mass.

1 INTRODUCTION

The self-gravity of a massive protoplanetary disc may, under certain conditions (Toomre 1964), cause small perturbations within the disc to grow in amplitude (i.e., a gravitational instability; GI) until the instabilities saturate in the non-linear regime. GIs can manifest themselves as spiral arms and shocks, heat the disc, and drive angular momentum and mass transport (see Durisen et al. 2007, for a review), as well as create molecular abundance variations that could be used as observational telltales of active GIs (Ilee et al. 2010, Douglas et al. 2013). If the combination of disc heating and mass transport fail to saturate (self-regulate) GIs (e.g., Gammie 2001; Cossins et al. 2009), then the densest regions of spiral arms can collapse to form self-bound gaseous clumps, which may be precursors of giant planets (e.g., Kuiper 1951; Boss 1998).

When such fragments first form, their mass is of order the mass of a gas giant planet (e.g., Boley et al. 2010; Nayakshin 2010b; Forgan & Rice 2011). However, their internal properties are very far from present day gas gi-

ants. In particular, the fragments are ~ 10 -12 orders of magnitude less dense than Jupiter(!), dominated in mass by molecular hydrogen, have initial central temperatures of just a few hundred Kelvin, and do not have high-metallicity cores (although they do contain an admixture of heavy elements and grains, perhaps significantly enriched over nebular abundances, see, e.g., Boley et al. 2011). Removal of gas by tides (Boley et al. 2010; Nayakshin 2010a) or the accretion of gas (Stamatellos & Whitworth 2008; Kratter et al. 2010) and planetesimals (Helled et al. 2006), plus nonlinear planet-disc coupling through radiative heat exchange (Vazan & Helled 2012; Nayakshin & Cha 2013) together make it extremely difficult to say what becomes of the remaining object. The list of possibilities goes from rocky and giant planets to brown dwarfs and even low mass stars (Stamatellos & Whitworth 2008; Kratter et al. 2010; Zhu et al. 2012; Forgan & Rice 2013).

Rapid inward migration of first fragments (Vorobyov & Basu 2005, 2006; Cha & Nayakshin 2011; Baruteau et al. 2011; Michael et al. 2011; Zhu et al. 2012) is a particular concern for the survivability of giant planets

formed by GIs. Initial fragment sizes are comparable to the corresponding Hill sphere of the clumps themselves, to within a factor of two or three (see, e.g., Boley et al. 2010). To survive the rapid radial migration, the clumps need to cool and contract rapidly, so that central temperatures reach ~ 2000 K (e.g., Helled et al. 2006) *before* tidal forces from the star disrupt the planet. At $T \sim 2000$ K, molecular hydrogen can dissociate, redirecting energy from pressure support into internal molecular processes. The resulting dynamical collapse of the protoplanet from sizes of $\sim 1000 R_J$ to a few to tens of R_J (Bodenheimer et al. 1980) is analogous to the end of the first core stage in star formation (e.g., Larson 1969), and may allow the protoplanet to avoid tidal destruction (e.g., Nayakshin 2010a).

In this paper we describe a second, so far insufficiently explored, channel for the collapse of giant planets faced with rapid inward migration. This second channel exists entirely due to the heavy element component within the fragments. As is well known, rapid grain growth can promote sedimentation of large grains to the centre of the clump (McCrea & Williams 1965; Boss 1998; Helled et al. 2008). In this paper we show that *if* the segregation of heavy elements to the central regions of the fragment is efficient, then dynamical collapse of the clump may be initiated by a dynamical instability in the clump’s centre, next to the core, *before the mean temperature of the fragment rises to ~ 2000 K*.

This instability is quite analogous to that laying the foundation of the core accretion plus gas capture theory of giant planet formation (e.g., Pollack et al. 1996), which we refer to as simply core accretion (CA) hereafter. In CA, the core grows by accretion of planetesimals from the disc and gravitationally attracts a gaseous “atmosphere”, again from the disc. The atmosphere’s mass increases as a steep power of core mass (Stevenson 1982). When the two masses become comparable, there is no stable hydrostatic solution and the atmosphere collapses onto the core dynamically (Mizuno 1980), triggering a rapid gas accretion from the disc onto the protoplanet (see Rafikov 2006, for a recent detailed treatment of the problem). We find a very similar sequence of events, except that the core grows by accretion of small grains rather than planetesimals, and all the action occurs inside a self-gravitating gas fragment born from GIs.

Understanding the core accretion-like instability discovered here is a key to understanding the pre-collapse evolution of the disc instability planets, and is necessary for identifying ways to distinguish observationally between planet formation modes. To differentiate between the instability discussed here and the one in the CA hypothesis, we call the collapse studied in this work a “core-assisted gas capture” (CAGC) instability, with emphasis that the core is embedded deep within a massive self-gravitating gaseous clump¹.

Global disc fragmentation simulations are not yet advanced enough to follow both the formation of a clump and the clump’s subsequent evolution to planetary scales. In particular, the region near the growing core is numerically challenging to investigate due to the required resolution and the

extreme changes in gas composition. For example, a core will have a radius of $\sim 10^{-4}$ AU, which is about 10,000 times smaller than the size scale of a molecular hydrogen gaseous clump. Although this core may be small compared with the total extent of the clump, we shall later see that destabilisation of gas directly surrounding the core can lead to collapse of the entire system.

Here, as a first step, we present a series of simple 1D models that focus on the structure of the gas atmospheres near cores that have a range of core properties (masses and luminosities). Our primary purpose is to address the following: (a) the conditions necessary for a core within a self-gravitating fragment to prompt dynamical collapse of the core’s atmosphere; (b) the critical core’s mass at which this collapse happens, and (c) the likelihood of these conditions to be met by fragments born from GIs within a reasonable protoplanetary disc setting. We present our numerical methods in section 2, and show the results of a case study for a particular clump mass in section 3. We then explore in section 4 the parameter space for which cores can drive the collapse of their atmospheres. Our results are summarised and their implications are discussed in section 5.

2 PHYSICS AND NUMERICAL METHOD

2.1 Relation to previous literature

The basic physics of core-assisted gas capture instability is very similar to that of the core accretion instability (e.g., Mizuno 1980). Consider a very dense core (solid or liquid) immersed in an initially uniform gas of a given (lower) density and temperature. Gravitational attraction of the core will pull gas layers closest to the core even closer, compressing the material, until a hydrostatic balance is established. At the same time, compression heats the material up, and since this all occurs on the (very short) local dynamical time scale, the compressed layer initially has an adiabatic structure. Perri & Cameron (1974) questioned hydrodynamical stability of the compressed gas, showing that when the core mass exceeds a critical value, M_{crit} , the layer becomes unstable due to combined core and self-gravity and will collapse to much higher densities. The critical core mass was found to be as high as $\sim 100 M_{\oplus}$ for conditions thought to be typical in the Solar Nebula (see also Wuchterl 1993).

However, two complications arise: (i) radiation diffusion may transport the compressional heat out, presumably decreasing the temperature of the compressed gas and hence M_{crit} too; (ii) On the other hand, the core may be a significant additional source of heat that acts in the opposite direction. A number of authors (Harris 1978; Mizuno et al. 1978; Mizuno 1980; Stevenson 1982) subsequently relaxed the assumption of adiabaticity for the gas in the envelope around the core. Assuming thermal energy equilibrium in the envelope instead, they obtained the critical core masses spanning a broader range from $\sim 1 M_{\oplus}$ to $\sim 100 M_{\oplus}$, depending on the outer boundary condition and opacity in the

¹ Hereafter, we refer to the gaseous region immediately surrounding a sedimented core as the core’s “atmosphere”, even though it is deep within a fragment’s interior.

envelope². See Rafikov (2006) and Hori & Ikoma (2011) for more recent studies of the problem.

These previous studies inform us here and shape our approach. A key difference between this work and what has been done previously is that we focus on massive clumps born by disc instability. Furthermore, we assume that dense cores readily form in these clumps as a result of grain settling. Strictly, the core formation timescale depends on the grain size distribution, but is estimated to be of the order of a few thousand to a few $\times 10^4$ years (Helled et al., 2008; Nayakshin, 2010), which we use in our calculations below. Within this context, we explore the hydrostatic stability of gas near the interface between the dense core and the gaseous envelope. Finally, for the calculations here, we do not simultaneously investigate the full evolution of fragments from their formation. Instead, we isolate the innermost region within evolved clumps (fragments) for which an embedded core has an immediate influence. We define this radius of influence as $r_i = GM_c/c_\infty^2$, where c_∞ is the gas sound speed at “infinity”, which is the bulk of the mass of a fragment. The region within r_i defines the atmosphere of the core, which is typically $r_i \sim 10^{-2}$ AU for core masses $\sim 10 M_\oplus$.

The presence of the envelope mass at $r > r_i$ is treated as an outer boundary condition. We assume that the gas fragment itself is not tidally limited. Because initial clump sizes can have radii over an AU in extent, our assumption of negligible tides implicitly assumes that the clumps are relatively far from their stars. Our calculations are relevant as long as the fragment is dominated by molecular hydrogen and does not fill its Roche lobe, which implies generally a distance to the host star of at least 1 AU or more, depending on the mass and age of the fragment (see, e.g., Nayakshin 2010a). As an example, for a 10^4 years old fragment of $2 M_J$, the corresponding orbital distance must be larger than ~ 10 AU.

In a fragment with radius $R \sim O(1AU)$, the gas density at $r_i \sim 0.01R$ is equal to the central clump density and is higher than the mean density. Tidal forces are thus negligible inside r_i . This is in contrast to the CA instability inside a protoplanetary disc, where the outer boundary of the gas atmosphere around the core can be set by the Hill’s radius.

2.2 Computational procedure

For simplicity, we assume a constant density for the core’s internal structure with $\rho_c = 10 \text{ g cm}^{-3}$, which reflects the expected density of giant planet cores (e.g., Guillot 2005). The sensitivity of the results to the chosen core density is investigated below, and found quite weak. The corresponding

² The absolute lower limit to the critical core mass is obtained (e.g., Sasaki 1989; Nayakshin 2011a) by assuming an isothermal structure for the envelope, $M_{\text{iso}} \approx 1 M_\oplus T_3^{3/2} (\mu/2.45 m_p)^{-3/2}$ where $T_3 = T_\infty/10^3$ K is the envelope’s temperature in units of 1000 K and μ is the mean molecular weight of the gas. This result is only pedagogically interesting, however, as the isothermal assumption is unrealistic for most conditions explored here: the cooling time within the dense envelope near the core can exceed the cooling time of the protoplanet itself and even the age of the Universe. Real systems will therefore never reach the isothermal solution and require larger M_{crit} .

core radius is given by $r_c = (3M_c/4\pi\rho_c)^{1/3}$. Because a fragment is not directly evolved in these models, and to reduce parameter space of our first study, we use the approximate formulae from Nayakshin (2010b,a) to describe gas density and temperature profiles at any given time t after the formation of a fragment, which can be used to derive initial conditions and boundary values. Eventually, we will incorporate the models presented here with simulations that also take into account the global evolution of clumps.

Our next steps are identical to what is done in CA studies except for the assumed core luminosity and atmosphere’s metallicity structure, as explained in §2.3 below. Starting with the boundary conditions from our evolved fragment models (actual evolution times given below), we integrate the equations of hydrostatic and energy transfer equilibrium inward from $r = r_i$ all the way to the core radius, $r = r_c$, using the standard procedure for atmospheric solution finding (e.g., see Hori & Ikoma 2011, for a recent treatment of the problem). In particular, the hydrostatic balance equation reads

$$\frac{dP}{dr} = -\frac{G(M_c + M_{\text{atm}}(r))}{r^2}\rho, \quad (1)$$

where M_c is the mass of the core, P and ρ are the gas, pressure, and density, respectively, and $M_{\text{atm}}(r)$ is the total mass of gas inside radius r . The gas includes an admixture of heavy elements.

Energy dissipation within the atmosphere itself is not included in these calculations. Although gravitational contraction will lead to a significant increase in a clump’s thermal energy over time, the energy released into the clump from gravitational work is deposited throughout the system, with only a small fraction deposited near the core. Since collapse of the material immediately surrounding the core (its atmosphere) occurs when its mass is of order the core’s mass and the atmosphere’s radial extent is a few to ten times that of the core (cf. figures 1 and 2 below), the total binding energy reservoir of this region must be considerably smaller than the binding energy of the core. This implies that converting the atmosphere’s binding energy into compressional heat is unlikely to result in luminosity exceeding that of the core, except perhaps for a short time. As a result, the luminosity that passes through the atmosphere is, to a good approximation, set by the luminosity of the core itself:

$$L_c = \text{const} = -\frac{64\pi r^2 \sigma_B T^3}{3\kappa\rho} \frac{dT}{dr}, \quad (2)$$

where ρ and T are the gas density and temperature at a distance r away from the core’s centre. Opacity coefficient κ is a function of gas density and temperature, and is taken from Zhu et al. (2009), which is an updated version of Bell & Lin (1994) opacities. The treatment of L_c will be discussed below. The energy transport mechanism in the atmosphere assumed in equation (2) is radiative diffusion. However, if the actual temperature gradient, $\nabla_{\text{rad}} = (P/T)dT/dP$, as calculated from equations (1) and (2), is larger than the adiabatic gradient (the convective stability criterion), ∇_{conv} , the temperature gradient is limited to $dT/dP = (T/P)\nabla_{\text{conv}}$.

The adiabatic temperature gradient is computed directly from the EOS of the mixture. The EOS we use was kindly provided by A.Kovetz and is similar to the one recently presented by Vazan et al. (2013). For hydrogen and helium the SCVH (Saumon et al. 1995) EOS is used, while

for lower pressures the EOS was extended based on the Debye approximation for a weakly interacting mixture. For the heavy elements, which are here represented by SiO_2 , the EOS is based on the quotidian equation of state (QEOS) described in More et al. (1988). The density of the mixture is calculated by applying the additive volume law, where the density of the mixture is determined by assuming that the volume of the mixture is the sum of the volumes of the individual components. The entropy of the mixture is the sum of the entropies of the individual components plus a term for the entropy of mixing (Saumon et al. 1995).

The equations of hydrostatic and energy balance just described allow us to integrate the density and temperature profile inwards all the way to the core’s boundary, provided that $M_{\text{atm}}(r)$ is known. This is not actually the case, and therefore iterations are required. Setting $M_{\text{atm}}(r) = 0$, we integrate the above equations from r_i to r_c once, and then repeat the procedure with $M_{\text{atm}}(r)$ calculated in the previous iteration. This procedure either converges to some finite value of the atmosphere’s mass, yielding a stable structure inside r_i – an atmosphere bounded by a massive envelope and a central core, or diverges, resulting in a runaway in the gas density and in the enclosed mass in the atmosphere. The largest value of M_c at which a stable atmospheric solution exists represents the critical core mass, M_{crit} .

2.3 Metal pollution and the critical core mass

Cores can grow at the centre of clumps through the sedimentation of small grains, e.g., \sim a few cm. In our previous work (e.g., Helled & Schubert 2008; Nayakshin 2010b, 2011a), these grains were assumed to accrete onto a core if they entered the innermost Lagrangian gas mass zone, below which the core is located. However, resolving the gas temperature profile closer to the core may invalidate this assumption since gas near the core is hotter. Grains evaporate rapidly when the surrounding temperature exceeds the grain’s vaporisation temperature, T_v , for the given material. Even for most of the refractory abundant grains, such as rocks, $T_v \approx 1400$ K (e.g., Podolak et al. 1988), with the rate of evaporation depending on grain size. As we show below, the temperature of the gas near the core is higher than 1400 K for all relevant parameter space considered, e.g., when the core mass increases above $\sim 1 M_{\oplus}$. We note in passing that this also implies that the dense cores of heavy elements that we study here are not necessarily solid. We simply assume that the core consists of heavy elements and that its density exceeds the surrounding gas density by orders of magnitude, and this is what matters for, e.g., setting the inner boundary of the atmosphere, r_c . Whether the core is solid, liquid, vapour, or (the most likely) a mix of these three phases is however important in determining the luminosity of the core, as discussed below.

When the core grows sufficiently massive, grains do not reach the core, but instead sediment down to the innermost region where $T > T_v$ and evaporate there. The heavy element content and hence the mean molecular weight of the gas around the core will increase above that of more distant regions (where $T < T_v$ and heavy elements continue to sediment as grains). We shall also see that the hot, inner, heavy-element-rich layer is usually strongly dominated by convection. Due to convective mixing, the heavy element

material in this region is well mixed with the gas throughout the convective layer, homogenising the heavy element content (cf. also Hori & Ikoma 2011).

Hori & Ikoma (2011) have used a similar setup to calculate the critical core mass in the context of the CA model for planet formation. It was found that the layer “polluted” by grains, formed in a way similar as described above, significantly reduces M_{crit} in the limit that the gas becomes dominated by heavy elements. In particular, M_{crit} may even fall below $1 M_{\oplus}$ for heavy element fractions of $z \gtrsim 0.8$ of the total gas mass. The main physical reason for such a behaviour is the increase in the mean molecular weight of the gas-heavy element mixture at high z (although latent heat, such as that due to evaporation of grains also helps to reduce M_{crit}).

A similar result is found here. However, we note that at very high- z , collapse of a relatively low-mass ($M \lesssim 1 M_{\oplus}$) heavy-element-rich layer onto the core does not, in general, mark the collapse of the entire fragment. The gas above the metal-polluted layer has metallicity much closer to the initial heavy element abundance of the gas, although depleted in accordance with the enrichment of the inner layers. The critical core mass for the gas with a Solar-like heavy element abundance is much higher. Therefore, collapse of the polluted heavy-element-rich atmosphere onto the core should strictly be considered as accretion of the inner layer onto the core. The accreting material is dominated by solids in this regime (because $z \rightarrow 1$), and only a small fraction ($1-z$) of it is hydrogen and helium. The collapse of the metal-polluted layer is thus effectively a delayed accretion of metals onto the core, which is not very different from a direct accretion of grains onto the core. Similar conclusions were reached by a number of authors in the context of CA model, although incoming high- z material there is in the form of planetesimals (e.g., Mordasini 2013). On the other hand, the luminosity of the core may be significantly different in these two pictures, as further discussed in section 2.4.

We thus arrive at the following phases of the core growth: (1) When the mass and the luminosity of the core is low, grain material is able to impact the core directly, as assumed in some previous studies. (2) When the core mass increases, eventually the gas near the core is hot enough to evaporate the grains. As a result, grains can evaporate before reaching the core. Their destruction simultaneously creates a heavy-element-polluted layer. As time progresses, the layer becomes completely dominated by high- z materials and can thus collapse onto the core, increasing its mass. Note that some H/He also accretes onto the core in this process. (3) As the core grows in mass, less heavy element pollution is required for the high- z layer to collapse. Eventually, layers with $z \sim 0.5$ are liable to collapse (this will be calculated below). At this point the core starts to gain as much mass in H/He as in metals, and this marks the beginning of rapid gas accretion onto the core.

Therefore, we define the critical core mass as one at which a moderately metal-polluted layer, $z = 0.5$, can collapse onto the core. After such a layer collapses, the increased mass of the core enables accretion of relatively metal-poor gas, $z < 0.5$, for which the presence of metals makes only a minor difference.

2.4 Core Luminosity

In this section we discuss the luminosity of the core, which can play a significant role in setting M_{crit} . In the core accretion model, it is customary to write

$$L_{\text{core}} = \frac{GM_c \dot{M}_c}{r_c}, \quad (3)$$

where \dot{M}_c is largely the planetesimal accretion rate onto a core. As discussed in the previous section, small grain accretion is necessarily complicated by grain evaporation and mixing with H/He in the heavy-element-polluted layer, which is also true in core accretion. Furthermore, when the heavy-element-rich layer does collapse onto the core, it is unclear how quickly the compressional heat gained in the collapse will escape from the core region.

These uncertainties are physically related to the difficult issue of determining how much heat is retained by gas that is accreted onto low-mass stars (e.g., Prialnik & Livio 1985; Hartmann et al. 2011) or onto giant planets (e.g., Marley et al. 2007). One can parameterise the energy retained per unit mass of accreted matter as $\alpha GM_c/r_c$, where α is an unknown factor between 0 and 1. Different values of α can lead to very different evolution histories, e.g., for stellar radius and luminosity in the two opposite limits (e.g., Prialnik & Livio 1985). When $\alpha \ll 1$, the accretion is called “cold”, and models that use these conditions have a “cold start.” When $\alpha \lesssim 0.5$ (as opposed to being very small, i.e., $\alpha \ll 1$), the accretion is “hot”, and corresponding models have a “hot start.”

While there are many similarities between core accretion and core sedimentation, there are also important differences. When core formation occurs within a gaseous clump as studied here, the core is buried deep in a very optically thick gas. As a result, the energy cannot be radiated away easily. To reflect this change, and the uncertain energy release rate under the accretion of heavy-element-polluted layers, we parameterise the energy loss from the core as

$$L_{\text{core}} = \frac{GM_c^2}{r_c t_{\text{kh}}}, \quad (4)$$

where t_{kh} is the Kelvin-Helmholtz contraction time of the solid core. The value of t_{kh} , which is taken to be a free parameter in our model, is varied over a broad range below.

Although the exact value of t_{kh} is unclear, there is a lower limit on t_{kh} imposed by the assembly time of the core. For example, compare equation (4) with equation (3), and let us also assume that all the accreted heat is being rapidly radiated away from the core. In this case t_{kh} should be replaced by the time scale on which the core grows, $t_{\text{growth}} = M_c/\dot{M}_c$, and the accretion luminosity given by equation (3) is recovered. From evolutionary calculations of fragments (e.g., Helled & Schubert 2008; Nayakshin 2010b), t_{growth} is from a few $\times 10^3$ to $\lesssim 10^5$ yr. For this reason, we take 10^4 yr as a rough representative cooling timescale. We do note that understanding the cooling timescale of clumps is an active area of research, with some groups finding, for certain conditions, very fast cooling times (Helled & Bodenheimer 2011).

On the other hand, the heat may be trapped inside the core for times much longer than t_{growth} . To explore a low-luminosity limit, we also consider values of t_{kh} in the range of 10^7 yrs.

3 AN EXAMPLE - 2 M_J FRAGMENT

We now consider an isolated gas clump of mass $M = 2M_J$ at time $t_{\text{age}} = 10^4$ yr from the fragment’s birth. This is motivated by the typical cooling time scale for the clumps, and is also consistent within an order of magnitude with the clump migration timescale into the inner disc (e.g., Nayakshin 2010a). The fragment is dominated by molecular hydrogen, so that the mean molecular weight at $r \geq r_i$ is set to $\mu = 2.45m_p$. The typical clump densities and temperatures in the centre of our clumps are estimated by using the analytical study of Nayakshin (2010b). In particular, we set the clump radius $R = 0.8$ AU ($t_{\text{age}}/10^4$) $^{-1/2}$. The temperature and mean density of the clump are then $GM\mu/(2k_B R)$ and $3M/(4\pi R^3)$, respectively. This yields gas density $\rho_\infty \approx 5.5 \times 10^{-10}$ g cm $^{-3}$ and temperature $T_\infty \approx 330$ K as the outer boundary conditions for our core atmosphere calculation. We plan to present more detailed time-dependent 1D models with different grain species in the near future.

Figure 1 presents the atmosphere structure for four different core masses, $M_c = 1, 3, 10$ and $45 M_\oplus$, shown with dot-dashed, dashed, dotted, and solid curves, respectively. All of these are computed in the limit of a relatively short t_{kh} , which we set to $t_{\text{kh}} = 10^4$ yrs. Panels (a) and (b) show the gas temperature and density structure, respectively. As expected, the atmosphere near the solid core becomes denser and hotter as M_c increases. Notice that the radial range of the atmosphere also increases. The inner boundary of the atmosphere, r_c , is proportional to $M_{\text{core}}^{1/3}$, resulting from the assumed fixed core density. The outer boundary $r_i \propto M_{\text{core}}$. Note the jump in density by about a factor of 2 in panel (b). This is the point where the metallicity of the gas is assumed to jump discontinuously from $z = 0.02$ ($T < T_v$, outer regions) to $z = 0.5$ ($T > T_v$), inner region. The gas temperature and pressure, $P = (\rho/\mu)k_B T$, are continuous across this transition, but the gas density ρ and the mean molecular weight μ are both discontinuous by the same factor across the kink.

Panel (c) of Figure 1 displays the ratio of the enclosed mass of the atmosphere, $M_{\text{atm}}(r)$, to the core mass, M_c . This ratio is found to increase strongly with M_c . The three lower core mass cases in Figure 1 show stable atmospheres that increase in mass proportionally with the core mass. The fourth case, which is the highest core mass case (solid curve), however, is qualitatively different. The atmosphere mass in this case is comparable to that of the core. At a core mass just slightly larger than $45 M_\oplus$, we find no static atmosphere solution; the atmosphere collapses dynamically. Therefore, the critical core mass in the $M = 2 M_J$, short t_{kh} , case is $M_{\text{crit}} = 45 M_\oplus$.

Figure 2 shows a very similar calculation but for a long t_{kh} case, $t_{\text{kh}} = 10^7$ yr. The core masses in this case are $M_c = 1, 3, 10$ and $12.5 M_\oplus$. By comparing Figures (2) and (1), it is found that the atmosphere is much more dense in the long t_{kh} case models, as expected: brighter cores require hotter atmospheres to transport the heat flux away. For this reason, the atmospheric collapse occurs at $M_c \approx 12.5 M_\oplus$, which is at a much lower core mass than in the short t_{kh} case.

To put these values of M_c in perspective, we note that a gas clump of mass $2M_J$ with solar [Fe/H] will have $\approx 12 M_\oplus$ of heavy elements. In order to get a core of $45 M_\oplus$ we need

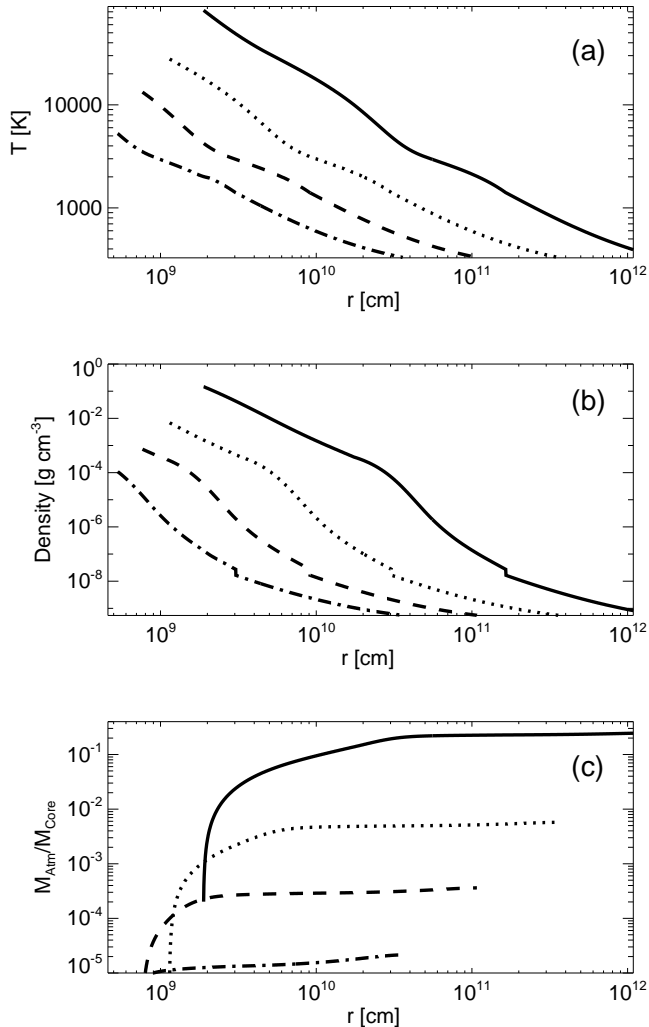


Figure 1. Structure of the atmosphere around cores of different masses in the bright core limit ($t_{\text{kh}} = 10^4$ years). The curves show gas temperature (panel a), gas density (b), and the enclosed mass $M_{\text{atm}}(r)/M_c$ (c). The core mass is $M_c = 1, 3, 10$ and $45 M_{\oplus}$ for the dash-dotted, dashed, dotted and solid curves, respectively. The discontinuity in density marks the division between the inner metal rich $z = 0.5$ atmosphere and the outer “normal” metal abundance gas, $z = 0.02$. There is no steady-state atmospheric solution for M_c larger than $45 M_{\oplus}$; the atmosphere collapses hydrodynamically.

a gas clump metallicity which is more than 3 times solar, or the clump needs to be significantly enriched relative to its birth nebula through, for example, planetesimal capture or gas-solid aerodynamic effects (e.g., Boley et al. 2011).

4 PARAMETER SPACE OF COLLAPSING ATMOSPHERE MODELS

We have illustrated the computational procedure with which we can determine the properties of the atmosphere of a heavy element core grown inside a fragment for a fixed set of properties, e.g., ρ_{∞} and T_{∞} . This procedure could be used in a fully self-consistent calculation for which the

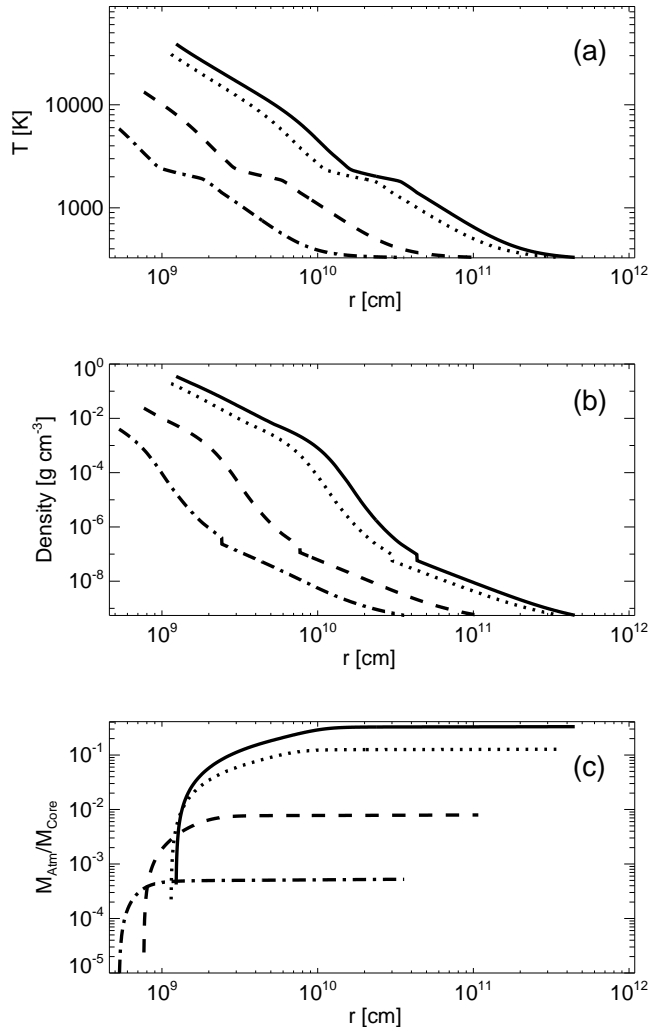


Figure 2. Same as Fig. 1, except in the dim core limit ($t_{\text{kh}} = 10^7$ years). The core mass is $M_c = 1, 3, 10$ and $12.5 M_{\oplus}$ for the dash-dotted, dashed, dotted and solid curves, respectively. There is no steady-state atmospheric solution for M_c larger than $12.5 M_{\oplus}$; the atmosphere collapses hydrodynamically.

properties of the gas clump and the rate of grain sedimentation are calculated as a function of time. The critical core mass then depends on the time evolution of the clump, and the value needed to induce collapse may or may not be reached. For example, the gas clump may contract and heat up too quickly for significant grain sedimentation and core formation to take place (Helled & Schubert 2008; Nayakshin 2010b).

In a yet more self-consistent calculation, the clump properties depend on its changing environment as it migrates inward. As noted in section 1, the clump may be even destroyed by tidal forces from the parent star (e.g., Boley et al. 2010; Nayakshin 2010a) or by overheating due to the thermal bath effect from the surrounding disc and stellar irradiation (e.g., Cameron et al. 1982; Vazan & Helled 2012) well before a core ever forms.

We have already implemented some of these model developments. However, the complexity and the parameter

space of such calculations are very large, and they fully deserve a separate future study. In this section we thus present a more modest approach in which we study isolated fragments that contract with time as prescribed by the simple analytical model of Nayakshin (2010a). This should provide a glimpse on how the critical core mass for atmosphere collapse scale with properties of the gas clumps, e.g., their masses. Such a mapping, together with the simple budget constrains on solids in a given clump, may allow us to make some *preliminary* conclusions as to when conditions needed for the atmosphere collapse can be realistically reached.

We use the same simple model, fixing the age of the gas clump at $t_{\text{age}} = 10^4$ yr as before, but we now consider a range of gas clump masses. Gas clumps much less massive than $\sim 1M_J$ are difficult to form in protoplanetary discs through fragmentation (e.g., Boley et al. 2010), while clumps more massive than $\sim 6M_J$ may be too hot at $t \sim 10^4$ yrs to allow grain sedimentation ($T_\infty > 1400$ K). For these reasons, we constrain our parameter search to be between 0.4 and 6 M_J . Figure 3 shows the critical core mass as a function of the total gas mass of the clump, M_{clump} , for several different values of the core cooling time, $t_{\text{kh}} = 10^4, 10^5, 10^6, 10^7$ and 10^8 yr, depicted by the solid curves from top to bottom, respectively. The highest luminosity case considered, $t_{\text{kh}} = 10^3$ yr is shown with a dot-dash red curve to distinguish it from the $t_{\text{kh}} = 10^4$ yr case.

The thin dash-dotted (blue) line on the bottom of the figure, marked "Isothermal", shows the isothermal critical core mass, M_{iso} , corresponding to the non-accreting and non-radiating core (e.g. Nayakshin 2011a). This $L = 0$ limiting case is non-realistic as gas cooling time near the surface of the core may be too long for the thermal equilibrium to be achieved (see the footnote in §2.1), but it is nonetheless instructive as an (analytical) absolute lower limit to M_{crit} . This line marks the estimated minimum critical core mass for a given temperature and density in the fragment (T_∞ and ρ_∞). $M_{\text{iso}} \propto T_\infty^{3/2}$, with a weaker dependence on ρ_∞ , this translates into a roughly $M_{\text{iso}} \propto M_{\text{clump}}^{3/2}$ scaling for the isothermal limit on the figure, given the simple Nayakshin (2010a) model for the gas fragment.

Figure 3 shows, as expected, that any $L > 0$ core ($t_{\text{kh}} < \infty$) requires a core mass larger than M_{iso} to enforce atmosphere collapse because the atmosphere around a luminous core is hotter. The least bright core case studied here, $t_{\text{kh}} = 10^8$ yrs, is the solid curve that gives the lowest values of M_{crit} . Analysis of atmospheric profiles of the respective models shows that the atmospheres on the flat part of the solid curves in fig. 3 (marked by "Part Radiative" in the figure) contain both convective and radiative regions. We should expect in this regime that the brighter the core is (the shorter t_{kh}), the more massive the core must be to cause the atmosphere to collapse. This trend is to be expected from the well known radiative zero solution for atmospheres (e.g., Stevenson 1982). The atmosphere mass scales as $M_{\text{atm}} \propto M_{\text{core}}^4/L$, so that higher L reduces M_{atm} at a given M_{core} . This explains why the critical core mass increases with decreasing t_{kh} on the flat part of the solid curves. The reason that the curves in this regime are almost independent of the clump mass, M_{clump} , is that the radiative zero solutions are dominated by regions very close to the cores, and are hence insensitive to ρ_∞ and T_∞ .

Sensitivity of M_{crit} to the core luminosity however becomes weaker and weaker as t_{kh} decreases, particularly for low-mass clumps. This is obvious from the top few solid curves in the figure, which become very closely spaced. In fact, models with $t_{\text{kh}} \leq 10^4$ yr saturate at a single curve (dash-dot red). The atmosphere of this limiting solution is fully convective, so that dT/dr is independent of L everywhere. The dash-dot red curve also marks this fully convective limiting solution. The solution corresponds to the fully convective, and thus adiabatic, atmospheres studied first by Perri & Cameron (1974), and also leads to very large values for M_{crit} . Considering the upper curves in figure 3, we find that the approximate relation $M_{\text{crit}} \approx 0.045M_{\text{clump}}$ matches the fully convective limit within $\sim 30\%$. The linear behaviour of M_{crit} with increasing M_{clump} can be obtained analytically by assuming that the atmosphere remains adiabatic with a constant specific heats ratio, γ (which is not exactly the case here, explaining why the curve is not quite linear).

The dotted thin lines in figure (3) are lines of a constant ratio $M_{\text{crit}}/M_{\text{clump}} = 0.005, 0.01, 0.02,$ and $0.1,$ from bottom to top, respectively. These lines are useful in determining the parameters of the clumps that may host a core that is massive enough to initiate a core-assisted gas capture (CAGC) instability at a given clump metallicity. If the curve (of a fixed t_{kh}) is above the line, then it is not possible to trigger CAGC for the given heavy element fraction and total clump mass, even if all the heavy elements sedimented into the core. For example, at half of the solar heavy element abundance (second from bottom dotted line), the maximum core mass would be $\sim 0.01M_{\text{clump}}$. Under these conditions, only gas clumps more massive than $\sim 3M_J$ could possibly provoke collapse and only if $t_{\text{kh}} = 10^7$ yr (second from bottom solid curve) or longer. If $t_{\text{kh}} \leq 10^6$ yr then no clump of this metallicity could ever collapse via the CAGC instability.

Evidently, assembling a core that is massive enough to induce atmosphere collapse is very difficult for systems that have low nominal heavy element fractions (i.e., low metallicity systems). Increasing the available budget of grains clearly improves the chances of reaching the critical core mass, creating a potentially strong dependence on heavy element abundance. Nonetheless, the exact form of this dependence is unclear from our study alone, and requires future additional work.

5 SENSITIVITY TO ASSUMPTIONS

5.1 Core density

In this paper we have assumed a fixed core density, $\rho_c = 10 \text{ g cm}^{-3}$. Density of the core could in principle be higher than this for very massive cores due to their large self-gravity. Alternatively, the core density could also be significantly lower than assumed here, especially for young hot cores (say, $t_{\text{kh}} \lesssim 10^4$ yr) which have not yet been able to radiate away the primordial heat of their formation. To test sensitivity of our results to the assumed value of ρ_c , we re-run some of the calculations presented in figure 3 for two additional values of core density, $\rho_c = 30 \text{ g cm}^{-3}$, and $\rho_c = 1 \text{ g cm}^{-3}$. Figure 4 shows the results of this experiment with the dotted and the dashed curves, respectively,

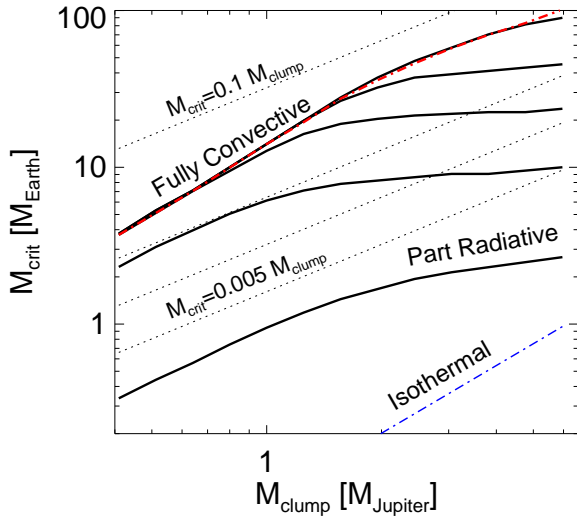


Figure 3. The critical core mass, M_{crit} versus the gas mass of the clump, M_{cl} , shown with thick curves. The five black solid curves are for different values of the core cooling time, $t_{\text{kh}} = 10^4, 10^5, 10^6, 10^7$ and 10^8 yr, from top to bottom, respectively. The thick dot-dashed (red) curve is same but for $t_{\text{kh}} = 10^3$ yrs. The dot-dashed (blue) line on the bottom shows the “isothermal limit”, $L = 0$ (see the footnote in §2.1). The power law dotted lines show constant $M_{\text{crit}}/M_{\text{clump}} = 0.005, 0.01, 0.02$, and 0.1 , from bottom to top, respectively. These lines reflect the minimum heavy element abundance required to initiate a CAGC instability. The red dot-dashed curve shows the limit at which the atmosphere becomes fully convective, which is why the curves become more closely spaced for higher core luminosities (small t_{kh}).

for these two values of the core densities. The solid curves reproduce the corresponding curves from figure 3.

We conclude that the dependence of M_{crit} on ρ_c is quite weak. An increase in ρ_c by a factor of three leads to at most a $\sim 10\%$ increase in the value of M_{crit} , whereas a ten-fold decrease in ρ_c decreases the critical mass by at most 30%. We interpret the insensitivity of the critical core mass to the value of ρ_c as being due to a near cancellation of two opposing effects. On the one hand, a denser core of a given mass commands a higher gravity, pulling the surrounding gas closer in and thus increasing the chance of the gravitational collapse of the atmosphere. On the other hand, a denser core also implies a higher luminosity (under the assumption of a fixed cooling time), since $r_c \propto \rho_c^{-1/3}$, which makes the collapse less likely as discussed in previous sections of the paper.

5.2 Dependence on collapse metallicity

A crucial argument was made in §2.3: the collapse of a *metal-dominated* atmosphere does not in general signal the beginning of a runaway *gas* accretion onto the core. Moreover, we argued that $z \sim 0.5$ (and not higher) is the critical metallicity for understanding the collapse of the entire system. This model assumption is in variance to Hori & Ikoma (2011) who suggested that critical core mass for core accretion in-

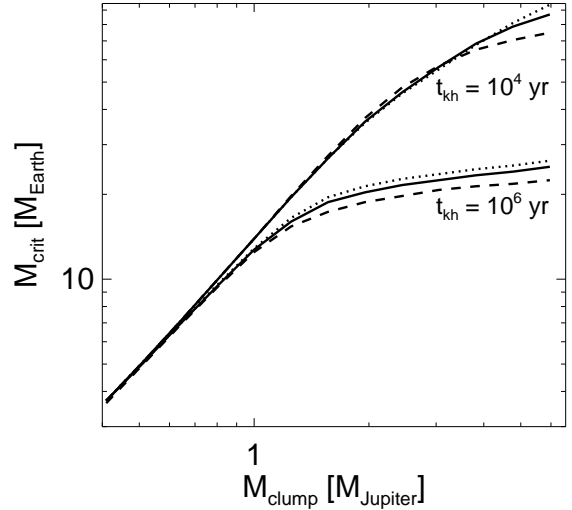


Figure 4. Sensitivity of the critical core mass, M_{crit} , to the core density. The solid curves are the same as the respective curves in Figure 3 ($t_{\text{kh}} = 10^4$ and 10^6 yr, as labelled on the figure). Recall that these two curves were computed assuming core density $\rho_c = 10 \text{ g cm}^{-3}$. The dotted and the dashed curves are for $\rho_c = 30 \text{ g cm}^{-3}$ and $\rho_c = 1 \text{ g cm}^{-3}$, respectively, with all other parameters the same as in the solid curves

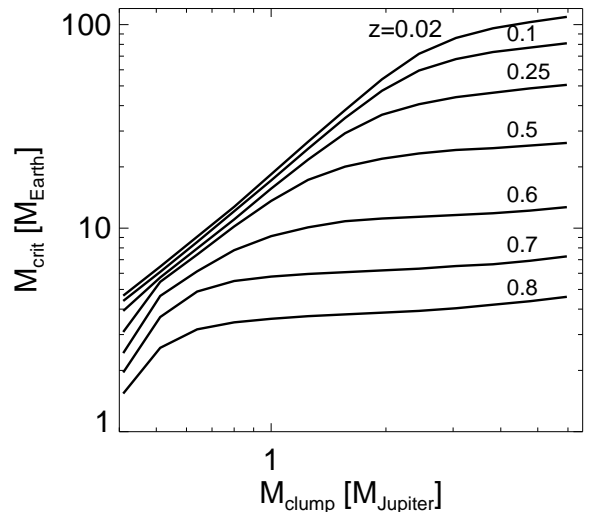


Figure 5. Sensitivity of M_{crit} to the critical metallicity that triggers atmosphere collapse. Note that for any clump mass, collapse of the atmosphere occurs for smaller critical masses as the metallicity of the gas is increased.

stability can be greatly reduced for strongly metal-polluted gas, so that M_{crit} is as small as $\sim (0.2 - 1) M_{\oplus}$ for $z \gtrsim 0.8$.

We test the sensitivity of our results to the metallicity z_{crit} of the atmosphere by varying the value of z_{crit} over a broad range. This also allows us to explore examples of systems for which the atmosphere should collapse, but the clump as a whole should not, as well as systems for which the instability of the atmosphere can drive the collapse of

the entire clump. Figure 5 shows a number of calculations identical to those done in §4, except just one particular core cooling time is used ($t_{\text{kh}} = 10^6$ yr) and the metallicity is varied from $z_{\text{crit}} = 0.02$ to $z_{\text{crit}} = 0.8$, as labelled on the figure.

Figure 5 confirms that higher metallicity gas is more susceptible to gravitational collapse (since M_{crit} is lower for higher values of z_{crit}). In this sense our results agree qualitatively with that of Hori & Ikoma (2011). However, our results also show that the collapse of a metal-dominated atmosphere does not obviously cause the collapse of the rest of the gas clump, which is assumed to have “normal” metallicity, e.g., that of the protoplanetary disc. To see this, consider the evolution of a growing, low-mass core, say $M_c \lesssim$ a few M_{\oplus} . Only a highly metal-polluted layer, $1 - z \ll 1$, could become gravitationally unstable around such a low-mass core. For definitiveness, consider $M_{\text{clump}} = 2M_J$ and $z = 0.8$ case, for which $M_{\text{crit}} \approx 4M_{\oplus}$. If the mass of the core roughly doubles when the whole metal polluted layer collapses onto the core (because such a collapse occurs when the mass of the metal-rich atmosphere is comparable to that of the core), we would have an $\sim 8M_{\oplus}$ core after the collapse. This is insufficient to induce collapse of the gas beyond the metal polluted layer. For the particular example at hand, a core mass of $\sim 55M_{\oplus}$ is needed to induce the further collapse of an atmosphere at $z \sim 0.02$. A new metal-polluted layer would have to build up, and that would collapse at $z \sim 0.67$ or so for $M_{\text{crit}} \approx 8M_{\oplus}$.

Collapse of the entire clump, however, seems to become possible if the instability in the atmosphere occurs at $z \sim 0.5$. For example, the critical core mass for such a “moderately” polluted atmosphere is $M_{\text{crit}} \approx 22M_{\oplus}$. If M_c does approximately double after this collapse, then even a normal metallicity gas, $z = 0.02$, becomes unstable to $M_{\text{crit}} \sim 50M_{\oplus}$. Collapse of a $z \sim 0.5$ atmospheric layer can thus potentially start the collapse of the gas fragment itself. Earlier collapses of metal-dominated layers should be interpreted as *core accretion*, albeit delayed and with some hydrogen rather than a true beginning of the gas accretion runaway phase.

5.3 Dependence on the metallicity-opacity coupling

We have used the opacity of Zhu et al. (2009) in this paper up to now, which includes dust, molecular, atomic, and electron scattering opacities in a tabulated format. Unfortunately, these tables assume the single (Solar) metallicity value, $z = 0.02$. The grey opacity can be much higher for a higher metallicity gas. For example, for dust opacity, a simple approximation is to assume that the opacity is directly proportional to the gas metallicity (although changes in opacity due to grain growth could render this approximation questionable Helled & Bodenheimer 2010).

Clearly, M_{crit} does depend on the opacity that is used, and it is important to at least estimate how strongly. Following grain growth and chemistry in detail is beyond the scope of this paper. Instead, we adopt the simple approach and assume that the grey opacity is directly proportional to z . In particular, we multiply all the opacity sources from Zhu et al. (2009) by the factor $z/0.02$, except electron scattering, which is only important at very high T .

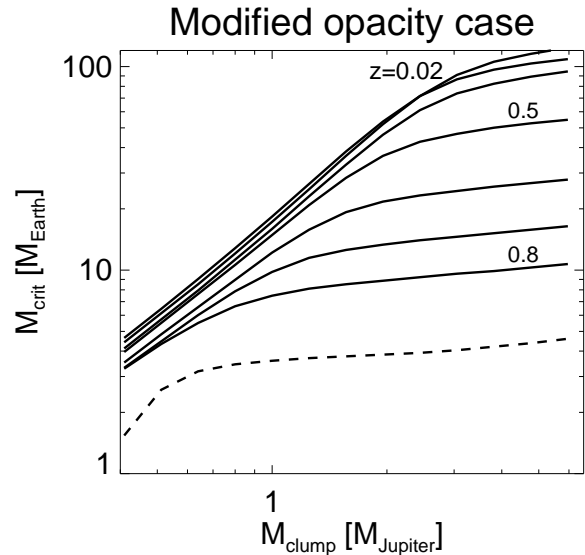


Figure 6. Same as Figure 5 but assuming that opacity in the metal-polluted layer is proportional to the metallicity of the gas (see text for more detail). The dashed curve is the $z = 0.8$ curve from Figure 5, shown here for comparison. The opacity does have an effect on the critical core mass required to induce collapse. However, this effect is limited to about a factor of two for the high-metallicity case.

As done in Figure 5, Figure 6 explores the model $t_{\text{kh}} = 10^6$ yr as a function of the metallicity of the polluted layer, but now with the increased opacities, as described above (solid curves). The same range of values for the layer’s metallicity is used in both figures. The dashed curve is the $z = 0.8$ model from Figure 5 plotted again for comparison.

We see that increasing the opacity increases the critical mass for collapse of the atmosphere, consistent with one’s intuition and with the more detailed study of Hori & Ikoma (2011). Fortunately, this increase in M_{core} is relatively small, e.g., only by a factor of ~ 2 for the highest metallicity case, in which the opacities were increased by the factor of $z/0.02 = 40$. This shows that opacity is indeed important in regulating the critical core mass, but less so than the metallicity of the metal-polluted layer. We draw a parallel here with previous work of Ikoma et al. (2000) who found that the critical core mass for atmosphere collapse in the CA theory scales as a very weak power-law of the opacity: $M_{\text{crit}} \propto k_{\text{gr}}^s$, where $s = 0.2 - 0.3$. Value of $s = 0.2$, in particular, is consistent with the increase of M_{crit} by a factor of 2 as opacity increases by a factor of 40. The physical reason for this behavior appears to be the fact that most of the atmosphere’s mass is located rather close to the core, where gas densities are very high (see e.g., figure 2), so that the convective rather than the radiative energy flux dominates.

5.4 Dependence on the age of the fragment

Finally, our standard value for the age of the gas clump was set to $t_{\text{age}} = 10^4$ yr so far. This is a reasonable estimate for the gas fragment migration time scale and the dust sedimentation time scale within the clump. However, a gas fragment’s thermal evolution may be affected by irradiation

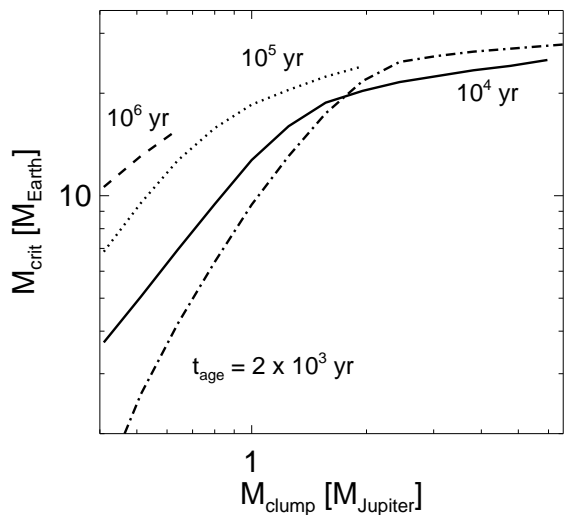


Figure 7. Same as figure 5 but assuming four different gas fragment ages, as marked on the figure next to the corresponding curves. The age of the clump has a very strong effect on the critical core mass, as the central properties of the clump vary significantly with time. Three of the curves do not cover the full range of clump masses because the central temperatures exceed the dust evaporation temperature for more massive clumps (at the given time).

tion from the surrounding disc and the parent star (e.g., Vazan & Helled 2012), and the migration time may vary depending on the disc properties (e.g., Nayakshin 2010a). Hence it is prudent to ask how our results depend on the age of the clump.

Figure 7 presents the critical core mass as a function of gas clump’s mass, M_{clump} , for just one value of $t_{\text{kh}} = 10^6$ yr, but for four different values of t_{age} , from 2×10^3 yr to 10^6 yr. The dominant effect seen in the figure is due to the contraction (and corresponding heating) of the clump with time. For example, clumps with a mass higher than $M_{\text{clump}} \approx 0.6M_J$ are hotter than 1400 K in the simple model of Nayakshin (2010a), so that grain sedimentation and core growth is not possible at this time. This is why the dashed curve continues only to this mass; higher mass clumps of this age would be too hot to continue accreting cores by grain sedimentation.

This figure, along with the standard parameter search shown in Figure 3, demonstrates that the internal structure of the gas fragment – controlled primarily by the clump’s mass *and* age – changes the critical mass M_{crit} most strongly. Future detailed investigations coupling the gas clump with the disc are required.

6 DISCUSSION

6.1 Main results of the paper

We used a series of 1D simple hydrostatic structure models to explore the stability of heavy element-rich atmospheres surrounding cores that are embedded deep within gaseous clumps. The clumps are envisaged to have formed through

the fragmentation of gravitationally unstable protoplanetary discs, while the cores are assumed to have formed through grain sedimentation. Our calculations show that the core’s atmosphere, i.e., the gas immediately surrounding the core, can become unstable and collapse for a range of fragment and core masses, as well as core luminosities. While the collapse of a core’s atmosphere in and of itself does not immediately imply that the entire clump will be unstable, experiments with the 1D radiation hydrodynamical code presented in Nayakshin (2011a, 2010a) did lead to the whole gas clump collapsing on a dynamical time scale for a few test problems explored. Since such a clump collapse is driven by H₂ molecule dissociation and H atom ionisation presenting very large energy sinks it seems reasonable to expect the whole clump collapsing once core atmosphere/envelope becomes unstable. This suggests that a disc fragment could form a gas giant planet via a novel channel that is discovered here. Namely, traditionally giant planet formation by gravitationally unstable discs is believed to occur via radiative cooling and contraction of self-gravitating gas fragments (see the review by Helled et al. 2013). Dust plays a passive (albeit important) role in this traditional picture by providing and regulating the opacity of the fragment (e.g., Helled & Bodenheimer 2010). In the picture developed in our paper, however, the dust plays a dynamically important role. By accumulating into a massive dense core in the centre, dust may provide a significant destabilising effect onto the whole gas fragment. This newly discovered core-assisted gas capture instability (CAGC) is closely linked to the well known Core Accretion instability (Mizuno et al. 1978; Harris 1978; Mizuno 1980; Stevenson 1982; Pollack et al. 1996; Rafikov 2006).

To enable a quantitative study of the CAGC, we made a number of model choices and simplifying assumptions. The gas fragment is assumed to be isolated from external influences and its structure is approximated by a very simple analytical model of Nayakshin (2010a). The dense core has a fixed density and its luminosity is given by the binding energy divided by a cooling time, t_{kh} , which is an important free parameter. The region closest to the core is metal polluted in our model since grains vaporise when $T > T_v = 1400$ K. We argued that gas fragment collapse can be triggered only if metallicity of the polluted layer is $z \lesssim 0.5$ as opposed to the limit $1 - z \ll 1$. Within these assumptions, our main quantitative results are as follows:

(i) The critical core mass, M_{crit} , that triggers the collapse of a core’s atmosphere is dependent most strongly on the central density and temperature of the fragment, as well as the luminosity of the core. More luminous cores (which corresponds to shorter t_{kh}) have more tenuous atmospheres, as expected, and hence brighter cores must be more massive to provoke the collapse (see fig. 3). As a numerical example, in a $2 M_J$ clump of 10^4 years of age from its birth, a core mass greater than $\sim 45 M_{\oplus}$ is required to cause collapse if the cooling time of the core is 10^4 yr. “Only” $M_{\text{crit}} \approx 12.5 M_{\oplus}$ is however needed for a cooling time of $t_{\text{kh}} = 10^7$ yr.

(ii) Since protoplanetary discs seem to disappear on time scale of order a few Million years, the most interesting value of t_{kh} to explore is of order 1 Million years or less (see §6.2 below on this point). The critical core mass is then (fig. 3)

between ~ 5 and $\sim 50 M_{\oplus}$, depending on properties of the gas fragment.

(iii) Less massive and younger gas fragments require smaller M_{crit} at the same t_{kh} (cf. figures 3 and 7).

(iv) Atmospheres of bright (short t_{kh}) cores are convective, whereas atmospheres of dim (long t_{kh}) cores are at least partially radiative. For our default opacity, the atmospheres become completely convective at cooling times of $\lesssim 10^4$ yr. In this case, the critical core mass is a function of the central pressure and temperature in the clump. At a given clump age and a clump opacity law, these are a function of the total clump mass, so the critical core mass becomes insensitive to the core luminosity/cooling times in the limit of shortest t_{kh} (cf. the upper enveloping (red) curve in figure 3).

(v) M_{crit} is very weakly dependent on the core density and opacity in the envelope (§§5.1 and 5.3).

(vi) The collapse of gas fragments to much higher protoplanetary densities via CAGC is strongly dependent on the availability of heavy elements, as larger critical core masses can only be reached for high initial metallicity. *Therefore, based on these results, a strong positive correlation between frequency of giant planets and metallicity may be expected with CAGC.* Low metallicity environments may be dominated by clumps that undergo collapse through H_2 dissociation.

6.2 Implications for the disc instability model

In the disc instability paradigm (e.g., Kuiper 1951; Boss 1997; Durisen et al. 2007), gas fragments of a few Jupiter masses are born in the outer cold and massive disc due to self-gravity instability. These fragments then cool and eventually collapse via hydrogen molecule dissociation in the fragment (Bodenheimer et al. 1980). Rapid inward migration of clumps (e.g., Vorobyov & Basu 2006; Cha & Nayakshin 2011; Baruteau et al. 2011; Michael et al. 2011; Zhu et al. 2012) may however lead to their destruction due to tides or irradiation (Cameron et al. 1982; Vazan & Helled 2012) or tidal disruption (Boley et al. 2010; Nayakshin 2010a). It is hence only those clumps that contracted before they were disrupted that may leave behind giant planets.

The newly found CAGC instability is an additional channel via which gas fragments may collapse. Dust growth and sedimentation into a core can be faster than the time taken by the fragments to cool to H_2 dissociation, especially for fragments less massive than a few Jupiter masses (Helled & Schubert 2008; Helled & Bodenheimer 2010; Nayakshin 2010b,a). Furthermore, such fragments are also most vulnerable to external irradiation which slows down their cooling even further (Vazan & Helled 2012). Therefore, CAGC may be the dominant channel through which such relatively low-mass fragments collapse to become giant planets.

We caution however that much more work is needed to test these ideas. Adding a self-consistent evolutionary model for the internal structure of a fragment interacting with the disc and the protostar and migrating inward is essential. In addition, there are several physical processes such as turbulence and magnetic fields which are not included in this work. These processes could affect the formation of clumps by gravitational instability and should be included in fu-

ture disc and planet formation models. Turbulence could also slow down formation of cores inside the fragments.

6.3 Implications for observations of giant planets

(i) Presence of a massive core. Based on the older variants of disc instability models (e.g., Boss 1997) that do not include planet migration and tidal stripping of the fragments, it is tempting to use the presence of a core in a gas giant as *prima facie* evidence of formation by core accretion plus gas capture, as core accretion *requires* the formation of a core (e.g., Mizuno 1980; Stevenson 1982; Pollack et al. 1996), while fragmentation by disc instability does not. However, as emphasized here, core formation could occur nonetheless through grain sedimentation (e.g., Boss 1997, 1998; Helled & Schubert 2008; Helled et al. 2008; Nayakshin 2010; Boley et al. 2010, 2011; Forgan & Rice 2013), and more importantly, if it does, can promote the collapse of the fragment if the core's mass exceeds M_{crit} . Sedimentation can hence erase or severely confuse using internal structure as evidence for a given formation mode, particularly if the formation of a heavy element core in a fragment can also lead to variations in final bulk composition, as discussed next.

Since the presence of a core can be explained by both formation scenarios it becomes harder to discriminate among the two models based on the core's mass. While it is still widely believed that small cores are more consistent with disc instability while massive cores are a natural outcome of core accretion, we found in this paper that reality may be much more complex. Even the extreme cases (i.e., no core at all versus a very massive core) do not implicate the formation process directly. This is due to the fact that very massive cores can also form in the disc instability picture if enrichment from birth and/or planetesimal capture occur, while no or very small cores are not inconsistent with core accretion if core erosion takes place. We therefore suggest once more, that core mass should not be used as a proof for a given formation model. In addition, one has to keep in mind that core masses are inferred only indirectly from models of their interior structure (e.g., Miller & Fortney 2011; Podolak & Helled 2012). For extrasolar giant planets it is not currently possible to distinguish between the total heavy element enrichment and high core masses (e.g., Helled et al. 2013).

(ii) Planet composition. Planets born by disc instability are often assumed to have the same composition as their host stars. However, several processes can occur that could potentially alter this (e.g., see review by Helled et al. 2013). As discussed above, the formation of a core in a clump must simultaneously deplete the clump's envelope of heavy elements. If core-assisted gas capture has occurred prior to the loss of the clump's envelope during disc migration, then any gas that is lost to the disc through tides would be preferentially depleted in heavy elements. Any remaining planet could thus appear to be significantly enriched in heavy elements.

(iii) Giant planet frequency of occurrence in the inner fraction of an AU was found to be a strongly increasing function of metallicity of the host star (Fischer & Valenti 2005). This has been traditionally interpreted as evidence for formation of these planets via Core Accretion picture. Our results however show that metal rich fragments born by the disc insta-

bility are more likely to collapse via CAGC, and it is thus possible that the observed correlation could be recovered by this model as well (cf. §4 and point (vi) in §6.1). This result is potentially exciting, but further work is required to better understand the dependence of CAGC on metallicity. On one hand, high heavy element abundances implies higher opacities and longer overall clump cooling times and perhaps larger cores (Nayakshin 2010b). On the other hand, high initial abundances could prompt prodigious grain growth. While this should promote a faster core growth, it could also actually decrease the overall cooling time of the clump (e.g., Helled & Bodenheimer 2011). The uncertainty in opacity due to grain growth is however also a concern for the CA model (e.g., Movshovitz et al. 2010).

Despite these uncertainties, it seems unlikely for CAGC to be important for clumps more massive than a few to ~ 10 Jupiter masses, because such clumps are unable to form massive solid cores quicker than they heat up to vaporise their grains (Helled & Schubert 2008; Nayakshin 2010b). Therefore, even under most optimistic assumptions about the CAGC contribution to forming giant gas planets, it seems highly unlikely that CAGC could explain planet-metallicity correlation for planets more massive than ~ 10 Jupiter masses.

6.4 Implications for observations of sub-giant planets

“Modern” versions of the disc instability model, e.g., those that include core formation, fragment migration and disruption (e.g., Boley et al. 2010; Nayakshin 2010a) are multi-outcome valued due to a large number of physical processes operating. Due to these processes, results obtained here may have important implications for close in “hot” (planet-star separation $a \sim 0.030.3$ AU) sub-giant planets as well.

In the context of such modern models, these close-in planets could have formed by the same process of grain sedimentation within the gas fragments, but in one of the following two distinctly different scenarios:

(i) Hot rocky super-Earths or hot-neptune planets of mass M_p are assembled by grain sedimentation inside gas fragments *that are disrupted before H_2 dissociation* while $M_p < M_{\text{crit}}$. If $M_p \ll M_{\text{crit}}$, only a tiny gas atmosphere would be retained after the disruption. If $M_p \lesssim M_{\text{crit}}$, a more massive atmosphere is retained, so that the planet may be neptune-like in terms of bulk properties and composition. Tidal disruption of pre- H_2 dissociation fragments can occur at distances $R \gtrsim 1$ AU to tens of AU, depending on the internal state of the fragments. For reference, tidal density around the Sun is $\approx 10^{-7}$ g cm $^{-3}$. Cores are much denser, so they survive this disruption (Boley et al. 2010). If they migrate inward via type I migration to $a \sim 0.1$ AU then they could potentially explain the population of close-in sub-giant exoplanets.

(ii) In the other scenario, H_2 dissociation and fragment collapse do take place before the clump is tidally disrupted. This could be either because $M_p \geq M_{\text{crit}}$ (collapse via CAGC instability studied here) or because the fragment contracted sufficiently strongly for H_2 dissociation to take place (as in the classical picture of, e.g., Bodenheimer et al. 1980), when $M_p < M_{\text{crit}}$. The key point here is that such

a collapse still does not necessarily implies the survival of the giant planet for astrophysically interesting time scales. For this to be the case, the planet must stop migrating towards the star. In the opposite case, the whole giant planet may be completely lost when it is swallowed by the parent star, or, alternatively – if the planet contracts slower than it migrates inward – it may be tidally disrupted in the “hot region” (Nayakshin 2011b), $a \sim 0.1$ AU. In this last case just the core is left behind. In contrast to the picture discussed in (i) above, the migration of the planet in this case is via type II until the gas fragment is disrupted. Nayakshin & Lodato (2012) showed that this close-in tidal disruption process reproduces some close in features of FU-Ori outbursts seen around some young stars (Hartmann & Kenyon 1996).

7 SUMMARY

We showed that gas fragments born by disc instability in the outer cold protoplanetary disc may collapse in a novel way when a massive dense core composed of heavy elements builds up in the centre of the fragments. The new Core-Assisted Gas Capture (CAGC) instability may allow fragment collapse to higher densities faster than by the traditional cooling and contraction route (Bodenheimer et al. 1980), especially for gas clumps less massive than a few Jupiter masses. This may enhance survivability of rapidly migrating gas fragments as giant planets. While significantly improved and expanded follow-up calculations are needed, this new mode of giant planet formation may show a positive correlation with host star’s metallicity.

8 ACKNOWLEDGMENTS

We thank A. Kovetz for providing us with the table EOS for hydrogen/metals mix. Theoretical astrophysics research in Leicester is supported by an STFC grant. ACB’s support is provided by The University of British Columbia.

REFERENCES

- Baruteau C., Meru F., Paardekooper S.-J., 2011, MNRAS, 416, 1971
- Bell K. R., Lin D. N. C., 1994, ApJ, 427, 987
- Bodenheimer P., Grossman A. S., Decamp W. M., Marcy G., Pollack J. B., 1980, ICARUS, 41, 293
- Boley A. C., Hayfield T., Mayer L., Durisen R. H., 2010, Icarus, 207, 509
- Boley A. C., Helled R., Payne M. J., 2011, ArXiv e-prints
- Boss A. P., 1997, Science, 276, 1836
- Boss A. P., 1998, ApJ, 503, 923
- Cameron A. G. W., Decamp W. M., Bodenheimer P., 1982, Icarus, 49, 298
- Cha S.-H., Nayakshin S., 2011, MNRAS, 415, 3319
- Cossins P., Lodato G., Clarke C. J., 2009, MNRAS, 393, 1157
- Durisen R. H., Boss A. P., Mayer L., Nelson A. F., Quinn T., Rice W. K. M., 2007, Protostars and Planets V, 607–622
- Fischer D. A., Valenti J., 2005, ApJ, 622, 1102
- Forgan D., Rice K., 2011, MNRAS, 417, 1928

- Forgan D., Rice K., 2013, *MNRAS*, 430, 2082
 Gammie C. F., 2001, *ApJ*, 553, 174
 Guillot T., 2005, *Annual Review of Earth and Planetary Sciences*, 33, 493
 Harris A. W., 1978, in *Lunar and Planetary Institute Science Conference Abstracts*, vol. 9 of *Lunar and Planetary Institute Science Conference Abstracts*, 459–461
 Hartmann L., Kenyon S. J., 1996, *ARA&A*, 34, 207
 Hartmann L., Zhu Z., Calvet N., 2011, *ArXiv e-prints*
 Helled R., Bodenheimer P., 2010, *ICARUS*, 207, 503
 Helled R., Bodenheimer P., 2011, *ICARUS*, 211, 939
 Helled R., Bodenheimer P., Podolak M., et al., 2013, *ArXiv e-prints*
 Helled R., Podolak M., Kovetz A., 2006, *ICARUS*, 185, 64
 Helled R., Podolak M., Kovetz A., 2008, *Icarus*, 195, 863
 Helled R., Schubert G., 2008, *Icarus*, 198, 156
 Hori Y., Ikoma M., 2011, *MNRAS*, 416, 1419
 Ikoma M., Nakazawa K., Emori H., 2000, *ApJ*, 537, 1013
 Kratter K. M., Murray-Clay R. A., Youdin A. N., 2010, *ApJ*, 710, 1375
 Kuiper G. P., 1951, *Proceedings of the National Academy of Science*, 37, 1
 Larson R. B., 1969, *MNRAS*, 145, 271
 Marley M. S., Fortney J. J., Hubickyj O., Bodenheimer P., Lissauer J. J., 2007, *ApJ*, 655, 541
 McCrea W. H., Williams I. P., 1965, *Royal Society of London Proceedings Series A*, 287, 143
 Michael S., Durisen R. H., Boley A. C., 2011, *ApJL*, 737, L42+
 Miller N., Fortney J. J., 2011, *ApJL*, 736, L29
 Mizuno H., 1980, *Progress of Theoretical Physics*, 64, 544
 Mizuno H., Nakazawa K., Hayashi C., 1978, *Progress of Theoretical Physics*, 60, 699
 Mordasini C., 2013, *ArXiv e-prints*
 More R. M., Warren K. H., Young D. A., Zimmerman G. B., 1988, *Physics of Fluids*, 31, 3059
 Movshovitz N., Bodenheimer P., Podolak M., Lissauer J. J., 2010, *ICARUS*, 209, 616
 Nayakshin S., 2010a, *MNRAS*, 408, L36
 Nayakshin S., 2010b, *MNRAS*, 408, 2381
 Nayakshin S., 2011a, *MNRAS*, 413, 1462
 Nayakshin S., 2011b, *MNRAS*, 416, 2974
 Nayakshin S., Cha S.-H., 2013, *MNRAS*
 Nayakshin S., Lodato G., 2012, *MNRAS*, 426, 70
 Perri F., Cameron A. G. W., 1974, *ICARUS*, 22, 416
 Podolak M., Helled R., 2012, *ApJL*, 759, L32
 Podolak M., Pollack J. B., Reynolds R. T., 1988, *ICARUS*, 73, 163
 Pollack J. B., Hubickyj O., Bodenheimer P., Lissauer J. J., Podolak M., Greenzweig Y., 1996, *Icarus*, 124, 62
 Prialnik D., Livio M., 1985, *MNRAS*, 216, 37
 Rafikov R. R., 2006, *ApJ*, 648, 666
 Sasaki S., 1989, *A&A*, 215, 177
 Saumon D., Chabrier G., van Horn H. M., 1995, *ApJS*, 99, 713
 Stamatellos D., Whitworth A. P., 2008, *A&A*, 480, 879
 Stevenson D. J., 1982, *P&SS*, 30, 755
 Toomre A., 1964, *ApJ*, 139, 1217
 Vazan A., Helled R., 2012, *ApJ*, 756, 90
 Vazan A., Kovetz A., Podolak M., Helled R., 2013, *MNRAS*, 434, 3283
 Vorobyov E. I., Basu S., 2005, *ApJL*, 633, L137
 Vorobyov E. I., Basu S., 2006, *ApJ*, 650, 956
 Wuchterl G., 1993, *ICARUS*, 106, 323
 Zhu Z., Hartmann L., Gammie C., 2009, *ApJ*, 694, 1045
 Zhu Z., Hartmann L., Nelson R. P., Gammie C. F., 2012, *ApJ*, 746, 110